"H_2 PRODUCTION FROM METHANE PYROLISIS OVER COMMERCIAL CARBON CATALYSTS: KINETIC AND DEACTIVATION STUDY"

D.P. Serrano[1,2*], J.A. Botas[1,2], R. Guil-Lopez[1]

1 Chemical and Environmental Technology Department, ESCET, Rey Juan Carlos University, C/ Tulipan s/n, 28933 (Mostoles)-Spain

2 IMDEA Energía, C/ Tulipan s/n, 28933 (Mostoles)-Spain

Published on:

International Journal of Hydrogen Energy

Volume 34, Issue 10, May 2009, Pages 4488-4494

doi:10.1016/j.ijhydene.2008.07.079

[*] *Corresponding author*. Tel.: +34 91 664 74 50; fax: + 34 91 488 70 68
e-mail address: *david.serrano@urjc.es*

Abstract

Hydrogen production from catalytic methane decomposition ($DeCH_4$) is a simple process to produce high purity hydrogen with no formation of carbon oxides (CO or CO_2). However, to completely avoid those emissions, the catalyst must not be regenerated. Therefore, it is necessary to use inexpensive catalysts, which show low deactivation during the process. Use of carbon materials as catalysts fulfils these requirements.

Methane decomposition catalysed by a number of commercial carbons has been studied in this work using both constant and variable temperature experiments. The results obtained showed that the most active catalyst at short reaction times was activated carbon, but it underwent a fast deactivation due to the deposition of the carbon formed from methane cracking. On the contrary, carbon blacks, and especially the CB-bp sample, present high reaction rates for methane decomposition at both short and long reaction times. Carbon nanotubes exhibit a relatively low activity in spite of containing significant amounts of metals. The initial loss of activity observed with the different catalysts is attributed mainly to the blockage of their micropores due to the deposition of the carbon formed during the reaction.

Keywords: hydrogen production, methane decarbonization, carbon catalyst, carbon black, activated carbon, carbon nanotubes.

1. Introduction

Hydrogen demand is ever growing, not only for using it as reactant in traditional applications (component of synthesis gas and hydrogenation processes, for instance), but also to use it as energy carrier [1]. The shift towards a hydrogen economy has been forecasted to take place in the next decades, which will result in a strong increase in the demand for hydrogen [2]. Thereby, it is necessary a change in the current energy system, which involves the development of new and alternative energy sources. Accordingly, new routes for hydrogen production must be found. Water is the ideal source for hydrogen, although water splitting is a process still in the initial phase of development [3,4]. Other promising renewable source for hydrogen production is biomass. A number of bio-materials have attracted attention in the last years to produce hydrogen by reforming [5-7]. In this way, biomass fermentation leads to bioethanol, which can be subjected to reforming to provide an alternative hydrogen production route. However, the fast deactivation of the metal catalysts used in this reaction and the presence of other competitive reactions, which decrease hydrogen selectivity, impose severe limitations on this technology [8].

Therefore, alternative processes must be developed, and current sources, including fossil fuels, must be also taken into account to produce hydrogen in short-medium terms. Nowadays, methane/natural gas reforming (SMR) is the most common industrial process for hydrogen production, due to the optimization of the use of energy in the centralised version of this process which reduces the cost of hydrogen production [9]. It involves the endothermic transformation of methane and water into hydrogen and carbon oxides (CO and CO_2). Hydrogen production from steam reforming of natural gas consists of several stages: (i) endothermic catalytic reforming of methane at high temperature (1073–1173 K) to produce synthesis gas; (ii) low temperature catalytic water gas shift (WGS) reaction (450-530 K) to convert CO into CO_2; and (iii) separation of the H_2-CO_2 mixture using a pressure-swing adsorption (PSA) unit. The process includes other stages such as a stock desulphurization unit and a steam generation section. For hydrogen use in polymeric exchange membrane fuel cells (PEMFC), CO concentration must also be minimized (less than

10 ppm) because it strongly poisons the anode electrocatalyst (Pt or Pt-Ru). Finally, the growth of concern on the anthropogenic CO_2 emissions reduction is forcing to capture and storage the CO_2 produced in each stage. The economic and energy cost of these additional operations reduces the overall efficiency and interest of this process, increasing the price of the hydrogen produced by steam reforming.

Among the possible hydrogen production technologies, the catalytic methane decomposition ($DeCH_4$) fulfils those requirements [10-13], not accomplished by SMR:

$$CH_4\ (g) \rightarrow C\ (s) + 2\ H_2\ (g), \qquad \Delta H_{1073} = 90.1\ kJ/mol\ (CH_4) \qquad \text{Equation 1}$$

The methane decomposition is a moderately endothermic process, which yields hydrogen as only gaseous product. The $DeCH_4$ process does not include WGS and PSA stages or others CO_2 capture and storage steps, which considerably simplifies the process and brings near the economical cost of hydrogen compared to that of the SMR process [11,12]. Moreover, hydrogen production by catalytic decomposition of methane, not only reduces the CO_2 emissions, but it allows high purity hydrogen to be obtained, which is optimal for its use in fuel cell applications. If in the future hydrogen is obtained using this process at a commercial scale, large amounts of solid carbon will be also co-produced (Equation 1). Therefore, the development of new carbon applications is a key factor to consolidate $DeCH_4$ technology as a feasible method for producing hydrogen. The carbon uses will depend on its nature and properties [14].

Traditionally, methane decomposition has been performed using metal catalysts, mainly Ni-based catalysts, as a typical way to produce carbon nanofibers. If the aim of the process is nanofiber production, Ni-catalyst must be destroyed after the reaction, to recover the produced nanofibers deposited on the catalyst [15,16]. However, when the aim of the process is hydrogen production, the Ni-catalyst must be recovered. Then, Ni particles must be stabilised to avoid their sintering along the different reaction-regeneration cycles [17-19].

Muradov has analysed energetic and economical factors to develop the catalytic $DeCH_4$ process using carbon as catalyst [13]. Carbon catalysts are not expensive materials, hence no regeneration is

needed. The oxygenate groups usually present on the carbon surface are removed before reaching the methane decomposition temperature, avoiding the contamination of the produced hydrogen with CO or CO_2. Specific studies using a variety of carbonaceous materials [20], such as coal char [21], activated carbons [22] or carbon blacks [23], as catalysts in this process have been carried out. In all cases, catalyst deactivation is present as a major issue due to the high amounts of carbon formed from methane decomposition.

In this context, the present work has been focussed on the activity exhibited in hydrogen production by methane decomposition by a number of commercial carbon materials. The evolution of the catalyst activity along the reaction time has been analyzed in order to evaluate their deactivation. Both initial activity and deactivation rate have been related with the properties of the carbon catalysts.

2. Experimental

Carbon samples

A total of five commercial carbons were used as catalysts for hydrogen production by methane decomposition. The carbon materials were chosen having a wide range of properties in order to ascertain their influence on the reaction being investigated. Two samples from Cabot *Corp.* (Vulcan XC72 and Black Pearls 2000, named CB-v and CB-bp, respectively), having different textural properties, were used as representatives of carbon black. An activated carbon (AC) from Merck was used as a microporous reference material. The multi-wall nanotubes sample was obtained from Sun Nanotech., having a high metal loading (named MWNT). Finally, graphite (GRAPH) from Fluka was used as a highly crystalline carbon.

Carbon characterization

The textural properties of the catalysts were determined from N_2 adsorption/desorption isotherms at 77 K, obtained with a Micromeritics TRISTAR 3000 instrument. Previously, the samples were

outgassed at 200 °C overnight. The surface area was calculated by applying the BET equation, whereas the distribution between micropore and external surface area was evaluated using the t-plot method.

XRD patterns of the carbons were recorded on a Philips PW 3040/00 X'Pert MPD/MRD diffractometer using Cu-K_α radiation at a scan rate of 0.2 $^{o}\cdot s^{-1}$ in the 2θ range of 5°–60°. The order of the graphene planes in each carbon material was studied using the characteristic graphitic C (002) and C (101) peaks.

Thermogravimetric combustion tests of the carbon catalysts were carried out on a TA Instruments SDT 2960 thermal analyser. Samples (5-10 mg) were heated to 1000 °C at 10 °C $\cdot min^{-1}$ with flowing air at 100 $mL\cdot min^{-1}$.

Transmission electron microscopy (TEM) was used to determine the particle size and morphology of both fresh catalysts and produced carbons. The samples were crushed in an agate mortar, dispersed in acetone and dropped onto a holey carbon microgrid. Micrographs were recorded using a Philips Technai 20 microscope operating at 200 kV.

CH_4 decomposition tests

The catalytic activity of the commercial carbons was tested by thermogravimetric measurements, following the increase in the sample weight during the reaction, caused by the deposition of the carbon formed as a by-product in methane decomposition (Equation 1). These tests were carried out on a TG/DTA SDT 2960 TA Instruments thermal analyser. Catalytic CH_4 decomposition was performed at atmospheric pressure by passing a flow of 100 $mL\cdot min^{-1}$ of 10 % CH_4 in Ar, using about 30 μl of each catalyst (i.e. different weights for each carbon) placed in a ceramic pan (90 μl of capacity). Since high amounts of carbon deposits are produced as the reaction progresses, the free-volume available in the pan could be a limiting factor. As a consequence of keeping approximately constant the catalyst volume placed in the ceramic pan, and due to the existence of high differences between the densities of the carbon materials, significant variations were produced

regarding the initial catalyst weight, as it is shown in the data included in Table 2. Prior to the reaction, the catalysts were dried under N_2 flow until 250 ºC. After drying, the samples were purged under the flow of the reaction mixture at 50 ºC.

Two kinds of tests were carried out:

- Temperature programmed reaction tests were carried out with every catalyst by increasing the temperature in the range 50 - 1100 ºC, at a constant heating rate of 10 ºC·min^{-1}. The systems were then maintained at 1100 ºC during 90 min. Initial catalytic activity was determined for each catalyst using the threshold temperature (T_{th}, defined as the temperature at which the starting catalyst sample weight increases by 0.05 % due to the carbon deposition coming from methane decomposition).
- Isothermal tests at 900 ºC in order to determine the activity order and its evolution along the reaction time. In this case, an inert stream was passed through the sample during the heating step, being switched to the 10 % CH_4 in Ar mixture once the desired temperature is reached.

3. Results and Discussion

Properties of the carbon catalysts

The main properties of the carbonaceous materials selected for being tested as catalysts in methane decomposition have been summarized in Table 1.

The textural properties (BET, micropore and external surface areas) of the carbon samples have been determined from the N_2 adsorption-desorption isotherms (see Figure 1 and Table 1). According to these results, the carbon catalysts can be classified into three groups: low surface area (graphite), intermediate surface area (carbon nanotubes and carbon black "vulcan"), and high surface area materials (activated carbon and carbon black "black pearls"). In the case of the activated carbon sample, the isotherm is clearly of type I, according to the IUPAC classification, indicating it is a microporous material. However, the isotherm of the carbon black CB-bp shows a

more complex shape, exhibiting significant adsorption at low relative pressure due to the presence of micropores, but showing also a sharp increase at high relative pressure originated from interparticle porosity. The latter is related to the small particle size of this sample, which is within the nanometer range, as shown in the TEM images (Figure 2). Both CB samples are formed by nanoparticles, which are smaller in the case of the CB-bp material. Accordingly, this catalyst presents also a significant amount of external surface area. In contrast, the CB-v sample exhibits little microporosity, showing that it consists mainly of non-porous nanoparticles, whereas most of its surface area is related to the external surface of the latter. Multi-wall nanotubes present a small surface area, whereas this parameter is even lower for the graphite sample.

The results from the XRD measurements are shown as the ratio between two of the peaks typical of graphenic materials, C(002) at $2\theta = 26°$ and C(101) at $2\theta = 44°$ (Table 1). The value of the intensity ratio C(101)/C(002) is usually taken as inversely related to the order of the graphene sheets [24,25]. Thus, the highly ordered planes of the graphite (GRAPH), which are piled up, show a low value of this XRD peak ratio. On the contrary, strongly disordered materials having a high surface area, as it is the case of AC and CB-bp, present a XRD peak ratio close to 1.

The order of the graphene layers for each carbon material can be also evidenced in the TEM measurements. Figure 3 shows the micrographs corresponding to four of the commercial carbons, which are presented by their increasing graphene sheet order: a) activated carbon; b) carbon black "black pearls"; c) carbon black "vulcan"; and d) high metal loading muti-wall nanotubes. Highly disordered AC (Fig. 3-a) shows very small environments of ordered graphene layers, which can be distinguished just at high resolution TEM. CB-bp shows larger areas of graphene sheets than in AC, whereas concentric graphene planes, characteristics of carbon black, starts to be noticed in this sample (Fig. 3-b). In the case of CB-v, clearly visible concentric graphene layers can be observed in the TEM micrographs (Fig. 3-c). Finally, MWNT shows the typical carbon nanotube arrangement with a pore size about 6.5 nm (Fig. 3-d), which is determined by the particle size of the metal used for nanotube preparation. All carbons were graphene materials, and the average value of the

graphene layers spacing derived from the TEM measurements was very close to the crystalline graphite d-spacing (~ 3.4-3.5 Å).

Similar conclusions can be obtained when analyzing the results of the carbon combustion temperatures (Table 1), which follow the sequence: AC < CB-bp < CB-v < GRAPH. This order of combustion temperatures agrees well with the graphene layers order, which is an expected result since a higher temperature is assumed to be necessary for breaking down a more stable crystalline structure. Thus, this sequence follows almost the same trend as that of the graphene layers order determined by XRD or TEM. However, the MWNT sample is out of the combustion data sequence, probably due to the presence of high amount of metals (15 % w/w), that decrease the combustion temperature, as they catalyse the carbon combustion.

CH_4 decomposition over carbon catalysts

The results obtained in the methane decomposition tests carried out at constant temperature using these carbons as catalysts are shown in Figure 4 as plots of sample weight evolution (%) *vs.* time. The results obtained with the graphite sample has not been included as this material showed a negligible weight increase, indicating it is not active in methane decomposition at least at the temperature used in these experiments (900ºC). Likewise, the threshold temperature (T_{th}) value from temperature-programmed reaction tests evidenced that graphite becomes active when reaching temperatures greater than 900 ºC (Table 2). The negligible activity of the graphite sample can be interpreted as a consequence of its high order degree (absence of defects) and its really low surface area.

The weight increase curves show two stages for most catalysts, with a progressive reduction in the slope as the reaction progresses. This fact can be directly related with the catalyst deactivation as a consequence of the carbon formed from methane decomposition which is deposited on the catalyst. This effect is clearly visible in the case of the active carbon sample, which passes from being the most active catalyst at short reaction times to present and almost negligible activity at long reaction times. On the contrary, just a small change in the slope of the curve corresponding to the MWNT

sample occurs along the reaction time. These findings can be confirmed from the data included in Table 2, where the values of the reaction rate at different times are shown in addition to the amount of carbon deposited on each catalyst for a prolonged reaction time.

At short reaction times (t = 10 min), the activity order observed is as follows: AC ~ CB-bp > CB-v > MWNT. This order agrees well with that found when using temperature programmed conditions (Table 2). In this case, the threshold temperature (T_{th}) is the main parameter determining the catalytic behaviour: a low T_{th} indicates a high carbon activity, whereas a high T_{th} is associated to a low catalytic activity. In addition, this activity order is the same as that found in the literature for this kind of carbon catalysts in isothermal experiments carried out at 850 C [20,26]. In the present work, AC and CB-bp were the materials exhibiting the lowest threshold temperatures, fact that has partially been assigned to their high surface area, although the main variable determining the activity has been recently proposed to be the disorder degree present in the graphene layers [24,27]. These parameters seem to be also the main factors determining the activity in the experiments performed in the present work at constant temperature and short reaction times.

However, the order of activity is significantly modified when analyzing the reaction rates obtained at long reaction times (see Table 2). In this case, AC is almost inactive in the reaction, showing that it has been almost completely deactivated by the carbon formed by methane decomposition. Since the AC sample is a microporous material, this result can be interpreted as a consequence of the micropore blockage by the deposited carbon, as evidenced in the TEM images of the spent catalyst (not shown here). In previous works, the same hypothesis has been proposed to justify the fast deactivation showed by activated carbon catalysts [20,22]. In contrast, the MWNT sample keeps around 74% of its initial activity after 100 min of reaction, indicating this material is little affected by the carbon deposits at least under the conditions here employed. Nevertheless, the reaction rate obtained with MWNT at long reaction times is still well below that observed using the CB-bp sample. Although the latter presents a high value of micropore surface area, which is probably also deactivated by the carbon deposition, it possesses a high share of external surface area

as it is formed by nanoparticles. This external surface area is probably the reason of the high activity exhibited by this sample at long reaction times and of its slow deactivation. The combination of both high initial reaction rate and resistance to deactivation in the CB-bp sample explain the high value of the carbon deposited on this material after 150 min of reaction.

4. Conclusions

A wide range of activities and deactivation rates have been obtained when using different carbonaceous materials as catalysts for hydrogen production by methane decomposition.

At short reaction times, the activity is mainly determined by the overall surface area and the amount of defects present in the graphene layers of the catalysts. However, at long reaction times the deposition of high amounts of carbon formed from methane decomposition may cause a significant deactivation of the catalysts, mainly by blockage of their micropores.

While graphite is practically inactive, at least at the temperature used in the present work, due to its small surface area and high degree of graphene order, activated carbon is the material with the highest reaction rate at short times. However, the latter becomes almost completely deactivated at long reaction times as a consequence of carbon deposition as it is mainly a microporous solid. The sample of multiwall nanotubes was quite resistant to deactivation, although showing a relatively low activity in the whole range of reaction times investigated. Finally, carbon black samples present an intermediate behaviour with both high initial reaction rates and significant resistance to deactivation. The best combination of both parameters is obtained with the CB-bp sample due to its high overall surface area and disorder degree of the graphene layers (high reaction rates at short times) and large share of external surface area (resistance to deactivation by carbon deposition and high activity at long reaction times).

Acknowledgements

The authors wish to thank "*Comunidad de Madrid*" for its financial support to the PHISICO2 Project through the Programme of Activities between Research Groups (S-0505/ENE-404). RGL acknowledges the *"Spanish Ministry of Science and Education*" and the European Social Fund for a "*Ramon-y-Cajal*" contract.

References

[1] Rostrup-Nielsen T. Manufacture of Hydrogen. *Catal. Today* 2005; **106**: 293-296.

[2] Marbán G, Valdés-Solís T. Towarsd the Hydrogen Economy?. *Int. J. Hydrogen Energy* 2007; **32**: 1625-1637.

[3] Ikuma Y, Bessho H. Effect of Pt concentration on the production of hydrogen by TiO_2 photocatalyst. *Int. J. Hydrogen Energy* 2007; **32** (14): 2689-2692.

[4] Huang C, Tabatabaie-Raissi A, Muradov N. A thermochemical cycle for production of hydrogen and/or oxygen via water splitting processes. *PCT Int. Appl*. 2007: WO2007002614A2.

[5] Vagia ECh, Lemonidou AA. Thermodynamic analysis of hydrogen production via steam reforming of selected components of aqueous bio-oil fraction. *Int. J. Hydrogen Energy* 2007; **32** (2): 212-223.

[6] Westermann P, Jorgensen B, Lange L, Ahring B, Christensen CH. Maximizing renewable hydrogen production from biomass in a bio/catalytic refinery. *Int. J. Hydrogen Energy* 2007; **32** (17): 4135-4141.

[7] Kinoshita CM, Turn SQ. Production of hydrogen from bio-oil using CaO as a CO_2 sorbent. *Int. J. Hydrogen Energy* 2003; **28** (10): 1065-1071.

[8] Ni M, Leung, Dennis YC, Leung MKH. A review on reforming bio-ethanol for hydrogen production. *Int. J. Hydrogen Energy* 2007; **32** (15): 3238-3247.

[9] Scholz WH. Process for Industrial Production of Hydrogen and Associated Environmental Effects. *Gas Sep. Purif*. 1993; **7**(3): 131-139.

[10] Steinberg M, Cheng H. Modern and prospective technologies for hydrogen production from fossil fuels, *Int. J. Hydrogen Energy* 1989; **14**: 797–820.

[11] Steinberg, M. Fossil Fuel Decarbonization Technology for Mitigating Global Warming. *Int. J. Hydrogen Energy* 1998; **23**: 419–425.

[12] Poirier MG, Sapundzhiev C. Catalytic Decomposition of Natural Gas to Hydrogen for Fuel Cell Applications. *Int. J. Hydrogen Energy* 1997; **22**: 429–433.

[13] Muradov NZ, Veziroglu TN. From hydrocarbon to hydrogen-carbon to hydrogen economy. *Int. J. Hydrogen Energy* 2005; **30(2)**: 225-237.

[14] Otsuka K, Takenaka S, Ohtsuki H. Production of pure hydrogen by cyclic decomposition of methane and oxidative elimination of carbon nanofibers on supported-Ni-based catalysts. *Appl. Catal. A: Gen.* 2004; **273**: 113-124

[15] Audier M, Coulon M, Bonnetain L. Hydrogenation of Catalytic Carbons Obtained by Carbon Monoxide Disproportionation or Methane Decomposition on Nickel. *Carbon* 1979; **17**(5): 391-394.

[16] Venugopal A, Naveen Kumar S, Ashok J, Hari Prasad D, Durga Kumari V, Prasad KBS, Subrahmanyam, M. Hydrogen production by catalytic decomposition of methane over Ni/SiO_2. *Int. J. Hydrogen Energy* 2007; **32(12)**: 1782-1788.

[17] Villacampa J I, Royo C, Romeo E, Montoya JA, Del Angel P, Monzon A. Catalytic Decomposition of Methane over $Ni\text{-}Al_2O_3$ Coprecipitated Catalysts; Reaction and Regeneration Studies. *Appl. Catal. A: Gen.* 2003; **252**(2): 363-383

[18] Li Y, Zhang B, Tang X, Xu Y, Shen W. Hydrogen production from methane decomposition over Ni/CeO_2 catalysts. *Catal. Commun.* 2006; **7**(6): 380-386

[19] Guil-Lopez R, La Parola V, Pena MA, Fierro JLG. Hydrogen Production via CH_4 Pyrolysis: Regeneration of ex Hydrotalcite Oxide Catalysts. *Catal. Today* 2006; **116**(3): 289-297

[20] Muradov N, Smith F, T-Raisi A. Catalytic Activity of Carbons for Methane Decomposition Reaction. *Catal. Today* 2005; **102-103**: 225-233.

[21] Bai Z, Chen H, Li W, Li B. Hydrogen Production by Methane Decomposition over Coal Char. *Int. J. Hydrogen Energy* 2006; **31**: 899-905.

[22] Moliner R, Suelves I, Lazaro MJ, Moreno O. Thermocatalytic Decomposition of Methane over Activated Carbons: Influence of Textural Properties and Surface Chemistry. *Int. J. Hydrogen Energy* 2005; **30**: 293-300.

[23] Dunker AM, Kumar S, Mulawa PA. Production of hydrogen by thermal decomposition of methane in a fluidized-bed reactor-Effects of catalyst, temperature, and residence time. *Int. J. Hydrogen Energy* 2006; **31**: 473-484.

[24] Guil-Lopez R, Fierro JLG, Botas JA, Serrano DP. Study on the Factors Determining the Activity in the Hydrogen Production by Methane Decomposition over Carbon Catalysts. *In preparation*.

[25] Feret, FR. Determination of the crystallinity of calcined and graphitic cokes by X-ray diffraction. *Analyst* 1998; **123**: 595-600.

[26] Suelves I, Lazaro MJ, Moliner R, Pinilla JL, Cubero H. Hydrogen production by methane decarbonization: Carbonaceous catalysts. *Int. J. Hydrogen Energy* 2007; **32**: 3320-3326.

[27] Dufour A, Celzard A, Fierro V, Martin E, Broust F, Zoulalian A. Catalytic decomposition of methane over wood char concurrently activated by a pyrolysis gas. *Appl. Catal. A: Gen.* 2007, *in press*.

Figure Caption

FIGURE 1. N_2 adsorption-desorption isotherms at 77 K of carbon catalysts.

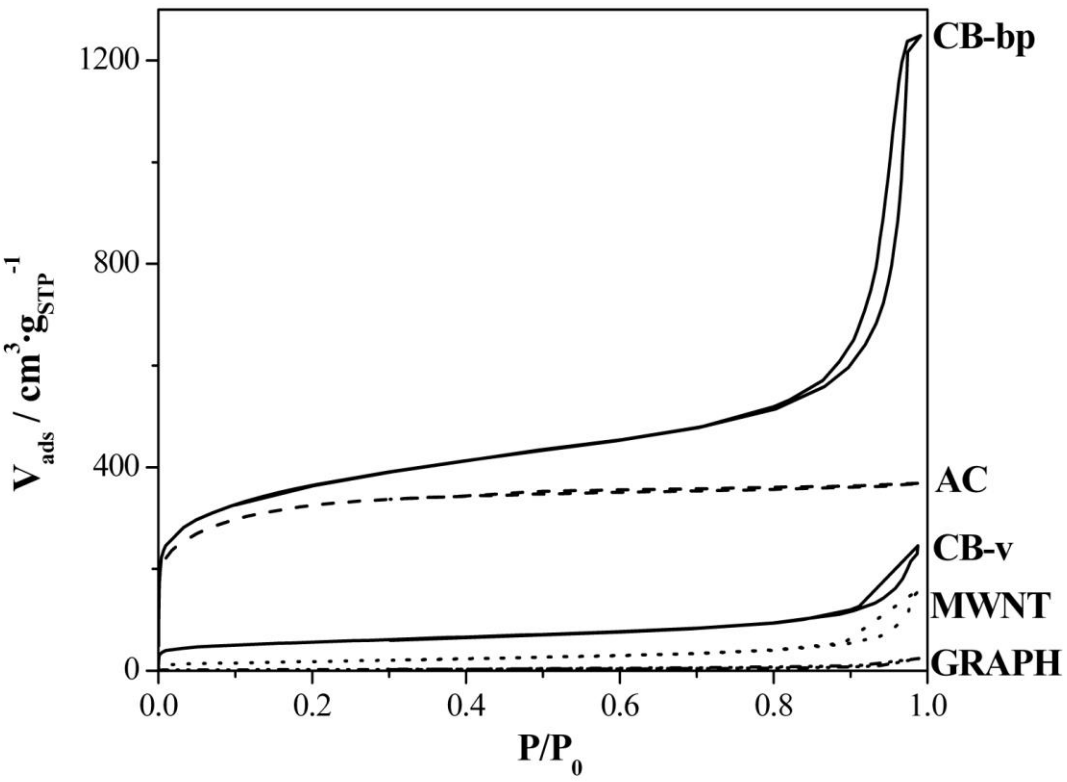

Figure 2: TEM images of carbon black catalysts: (a) CB-bp; and (b) CB-v.

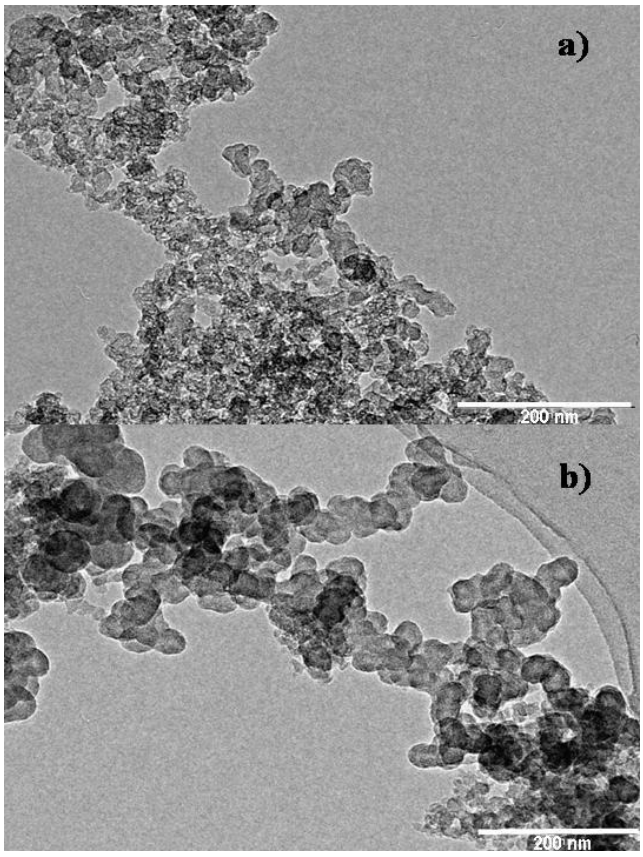

Figure 3: TEM images of carbon catalysts: (a) AC; (b) CB-bp; (c) CB-v; and (d) MWNT.

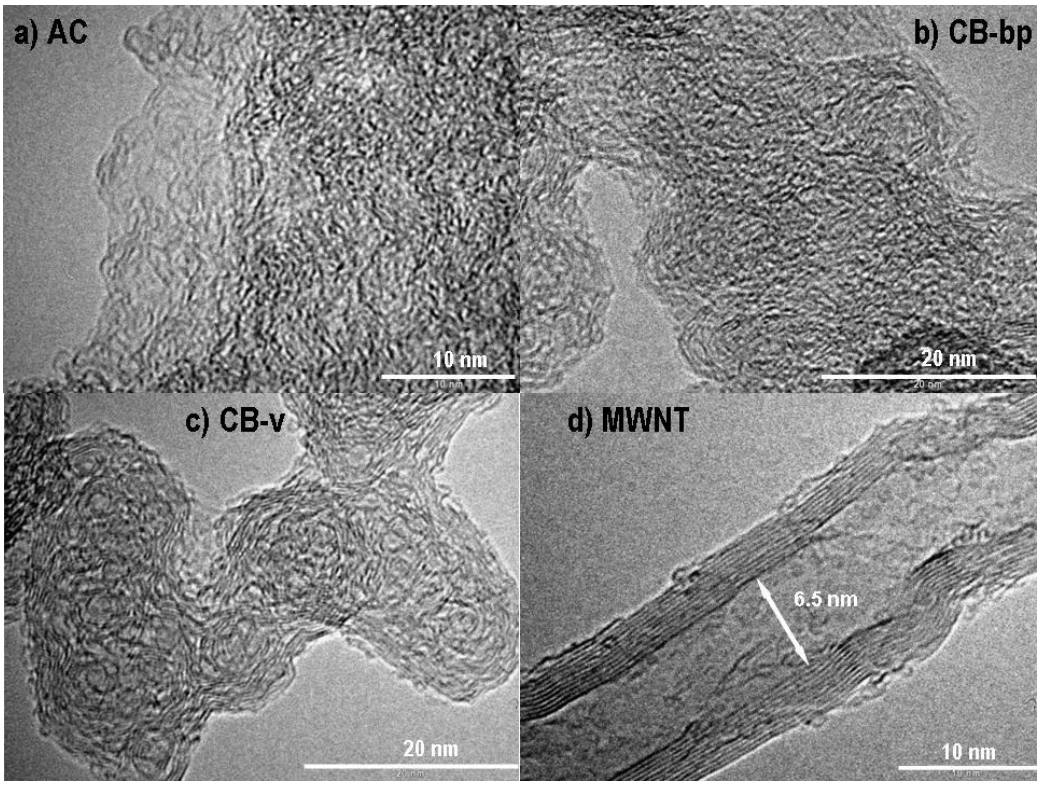

FIGURE 4. Methane decomposition catalyzed by carbon materials at 900ºC.

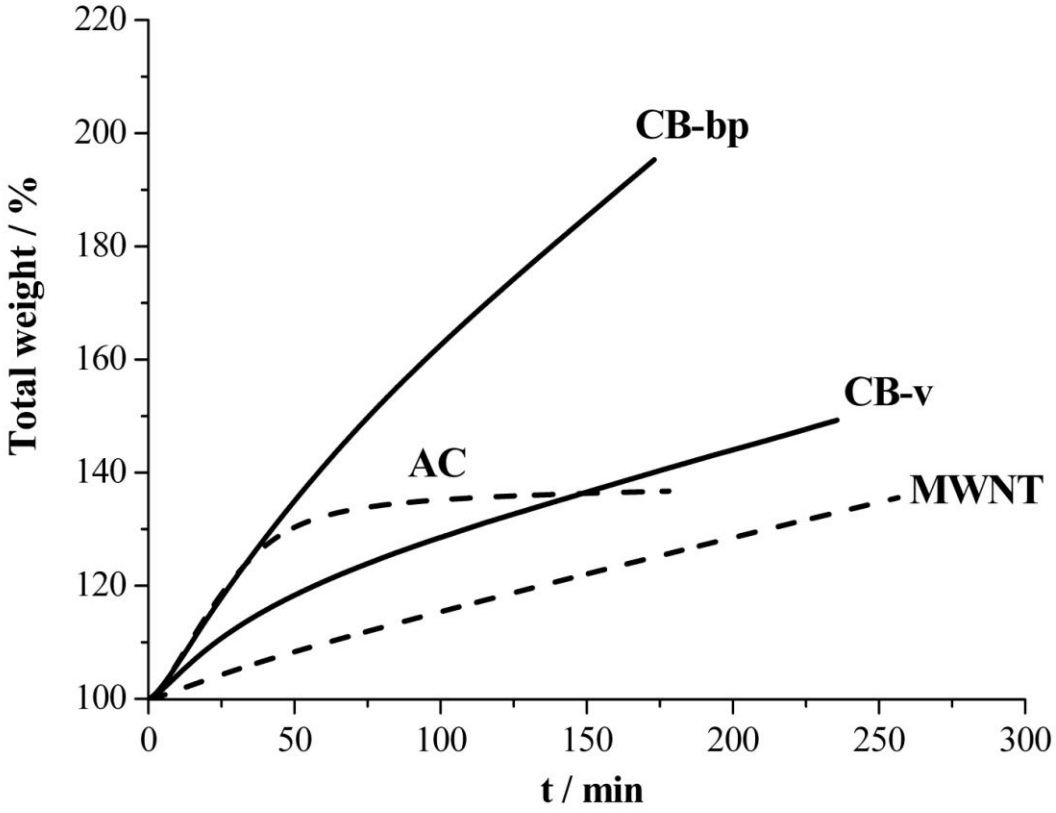

Tables

TABLE 1. Properties of the carbon catalysts.

Catalyst	Textural properties				XRD intensity ratios	T_{comb} [b] / ºC
	S_{BET} / $m^2 \cdot g^{-1}$	S_{EXT} / $m^2 \cdot g^{-1}$	S_{MIC} / $m^2 \cdot g^{-1}$	V_p [a] /$cm^3 \cdot g^{-1}$	C(101)/C(002)	
AC	1152	81	1071	0.57	0.84	605
CB-bp	1285	297	988	1.93	0.94	620/635
CB-v	196	168	28	0.38	0.65	665
MWNT	65	45	20	0.26	0.51	635
GRAPH	8	8	---	0.04	0.03	> 850

[a]Total pore volume at P/Po = 0.99.
[b]Combustion temperatures measured by TG analysis in air.

TABLE 2. Kinetic parameters derived from the catalytic experiments of methane decomposition.

Catalyst	Catalytic results					
	Isothermal tests (T = 900ºC)				Temperature-programmed tests	
	w[a]/mg	Produced carbon ($mg_{carbon} \cdot mg_{catayst}^{-1}$) t = 150 min	Reaction rate ($mg_{carbon} \cdot mg_{catayst}^{-1} \cdot min^{-1}$) t = 10 min	t = 100 min	w[a]/mg	T_{th} [b] / ºC
AC	13.9	0.36	0.0084	0.0004	11.9	779
CB-bp	4.10	0.85	0.0077	0.0049	4.41	778
CB-v	3.82	0.37	0.0049	0.0017	3.14	797
MWNT	4.10	0.22	0.0019	0.0014	3.41	869
GRAPH	---	---	---	---	10.0	905

[a] Initial weight of the carbon catalysts employed in the experiments.
[b] Threshold temperature (T_T), defined as the temperature at which the starting catalyst weight increases by 0.05 % due to the carbon deposition coming from methane decomposition.